Diagn Interv Radiol 2016; 22:407–421

CHEST IMAGING

REVIEW

Contrast-enhanced CT- and MRI-based perfusion assessment for pulmonary diseases: basics and clinical applications

Yoshiharu Ohno
Hisanobu Koyama
Ho Yun Lee
Sachiko Miura
Takeshi Yoshikawa
Kazuro Sugimura

ABSTRACT

Assessment of regional pulmonary perfusion as well as nodule and tumor perfusions in various pulmonary diseases are currently performed by means of nuclear medicine studies requiring radioactive macroaggregates, dual-energy computed tomography (CT), and dynamic first-pass contrast-enhanced perfusion CT techniques and unenhanced and dynamic first-pass contrast enhanced perfusion magnetic resonance imaging (MRI), as well as time-resolved three-dimensional or four-dimensional contrast-enhanced magnetic resonance angiography (MRA). Perfusion scintigraphy, single-photon emission tomography (SPECT) and SPECT fused with CT have been established as clinically available scintigraphic methods; however, they are limited by perfusion information with poor spatial resolution and other shortcomings. Although positron emission tomography with ^{15}O water can measure absolute pulmonary perfusion, it requires a cyclotron for generation of a tracer with an extremely short half-life (2 min), and can only be performed for academic purposes. Therefore, clinicians are concentrating their efforts on the application of CT-based and MRI-based quantitative and qualitative perfusion assessment to various pulmonary diseases. This review article covers 1) the basics of dual-energy CT and dynamic first-pass contrast-enhanced perfusion CT techniques, 2) the basics of time-resolved contrast-enhanced MRA and dynamic first-pass contrast-enhanced perfusion MRI, and 3) clinical applications of contrast-enhanced CT- and MRI-based perfusion assessment for patients with pulmonary nodule, lung cancer, and pulmonary vascular diseases. We believe that these new techniques can be useful in routine clinical practice for not only thoracic oncology patients, but also patients with different pulmonary vascular diseases.

Matched distribution of regional pulmonary blood flow (perfusion) and ventilation is required for pulmonary ventilation and perfusion assessment to proceed efficiently (1). A large amount of ventilation in lungs is matched by correspondingly high perfusion. In addition, the balance between pulmonary perfusion and ventilation differs according to the physiopathology of various pulmonary diseases, and the normal pattern of pulmonary blood flow often changes, sometimes exacerbating the disturbance in gas exchange (2, 3). Therefore, assessment of these regional perfusion pattern changes is important to understand the pulmonary pathophysiology of various pulmonary diseases. Multiple methods are currently available to quantitatively and qualitatively evaluate pulmonary perfusion in patients with pulmonary diseases.

Currently, regional pulmonary perfusion assessment for various pulmonary diseases as well as nodule and tumor perfusion assessments are performed by means of nuclear medicine studies (2–9), dual-energy (10–12) and dynamic first-pass contrast-enhanced perfusion computed tomography (CT) techniques (13–17), unenhanced and dynamic first-pass contrast-enhanced perfusion magnetic resonance imaging (MRI), as well as time-resolved three-dimensional (3D) or four-dimensional (4D) contrast-enhanced magnetic resonance angiography (MRA) (18–25). While perfusion scintigraphy, single-photon emission tomography (SPECT) and SPECT fused with CT (SPECT/CT) are established as clinically available scintigraphic methods, they are limited by factors such as perfusion information with poor spatial resolution. Moreover, absolute quantification of pulmonary perfusion by radionuclide scanning requires arterial sampling and correction for tissue attenuation of gamma radiation emitted by technetium-99m. Although positron emission tomography (PET) with ^{15}O water can measure absolute pulmonary perfusion (4), it requires a cyclotron for production of tracers with an extremely short half-life (2 min), and can currently be performed for limited academic and/or clinical purposes only. Clinicians are therefore concentrating

From the Division of Functional and Diagnostic Imaging Research, Department of Radiology and Advanced Biomedical Imaging Research Center (Y.O. ✉ *yosirad@med.kobe-u.ac.jp,* H.Y.L., T.Y.), Kobe University Graduate School of Medicine, Kobe, Hyogo, Japan; the Division of Radiology (H.K., K.S.), Department of Radiology, Kobe University School of Medicine, Kobe, Hyogo, Japan; the Department of Radiology (H.Y.L.), Sungkyunkwan University School of Medicine, Irwon-Ro, Gangnam-Gu, Seoul, Korea; the Department of Radiology (H.Y.L.), Samsung Medical Center, Irwon-Ro, Gangnam-Gu, Seoul, Korea; the Department of Radiology (S.M.), Nara Medical University, Kashihara, Nara, Japan.

Received 29 February 2016; accepted 1 March 2016.

Published online 12 August 2016.
DOI 10.5152/dir.2016.16123

their efforts on the application of CT- and MRI-based quantitative and qualitative perfusion assessment to various pulmonary diseases.

This review article covers 1) the basics of dual-energy CT and dynamic first-pass contrast-enhanced perfusion CT techniques, 2) the basics of time-resolved contrast-enhanced MRA and dynamic first-pass contrast-enhanced perfusion MRI and 3) clinical applications of contrast-enhanced CT- and MRI-based perfusion assessment for patients with pulmonary nodule, lung cancer, and pulmonary vascular diseases.

Basics of CT-based imaging techniques

Dual-energy CT

Dual-energy CT techniques using dual x-ray sources, dual-layer detectors, or fast kilovoltage-switching methods were introduced in the 1970s (24–26). However, several factors including insufficient tube technology and poor spatial and temporal resolutions have been identified as limitations of these techniques. In addition, misregistration between the low-energy and high-energy datasets seemed unavoidable. However, improvements in the dual-energy CT technique have made it possible to simultaneously obtain datasets for two different photon spectra with satisfactory image quality in a single CT acquisition. Moreover, recent technical advances in CT have resulted in the development of CT scanners with a dual-source system that are equipped with two x-ray tubes and corresponding detectors mounted with a particular angular offset (10, 11, 27, 28), a single-source CT system with ultrafast tube voltage switching at an x-ray tube and the corresponding detector (10, 11), and a single-source CT system with a constant tube current and voltage setting and a corresponding detector that can compartmentalize detected x-ray photons into energy bins (11, 28). The detector for these approaches comprises two layers, an upper layer that absorbs the lower-energy photons and a lower layer registering the remaining higher-energy emissions; from these two datasets, two separate image series are reconstructed and analyzed (11, 28).

Each tube operates independently with regard to tube voltage and tube current on the dual-source CT platform, and makes it possible to obtain one consisting of simultaneous registration of high- and low-energy x-ray spectra. On the other hand, ultrafast tube voltage switching on a single-source CT platform differs from dual-source CT-based dual-energy CT in terms of both image data acquisition and processing methods but has similar applications. However, this method is characterized by a very small temporal difference between acquired CT data from low-energy and high-energy x-ray spectra, no matter which ultrafast tube voltage switching is performed during ultrafast gantry rotation (29). In contrast to the abovementioned two approaches, a third method, which has a single-source CT with two layered detectors, has been developed, but is not yet available for routine clinical practice. Therefore, the dual-source CT system is most frequently used for dual-energy CT-based perfusion assessment in routine clinical practice. Although their CT system and data acquisition methods are different, all three methods make it possible to demonstrate iodine distribution maps within the lungs in patients with pulmonary vascular diseases (Fig. 1) as well as nodules and/or masses. With dual-energy CT, the attenuation of iodine is far greater at 80 kVp than at 140 kVp, so this technique can be used for evaluation of pulmonary diseases by means of virtual unenhanced images (10, 30, 31), which may obviate additional acquisition of actual unenhanced CT scans. Thus, a single contrast-enhanced acquisition can yield both unenhanced and contrast-enhanced CT data (10, 30, 31). The basic principle of dual-energy CT involves material decomposition based on attenuation differences at different energy levels (32). In the lung—as an example of the three-component system, consisting of air, soft tissue, and iodine—the algorithm assigns a ratio of air and soft tissue to the voxel. At the same time, CT data at both energy levels are used to derive the additional iodine content.

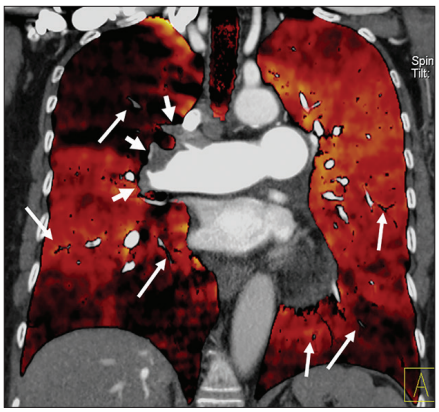

Figure 1. A 65-year-old female with pulmonary thromboembolism with right heart dysfunction. Color-coded lung perfused blood volume (Lung PBV) map and averaged CT image from 80 kVp and 140 kVp images of vasculature were fused by commercially available software. On fused image, thrombi in central zones *(large arrow)* and peripheral zones *(small arrows)* are clearly demonstrated as defects within pulmonary vasculatures. In addition, heterogeneously decreased perfusion within right upper and both lower lung fields are clearly demonstrated as Lung PBV map information. Dual energy CT can show not only morphologic, but also functional information on the same image.

Various image acquisition protocols for dual-energy CT by means of a few dual-source CT systems have been proposed in the literature (11, 33–36), but currently only a few published protocols are available for single-source CT systems (11, 33). Optimization of contrast medium injection parameters, including the use of a saline chaser bolus, can reduce artifacts, improve image quality, and increase diagnostic accuracy. High concentration of iodine contrast media (i.e., >300 mgI/mL) is recommended for dual-energy CT studies to improve the differentiation of iodine by means of dual-energy postprocessing algorithms. To evaluate both anatomical and functional information about pulmonary circulation (i.e., pulmonary vasculatures and perfusion), the scanning delay should be slightly longer (e.g., 4–7 s) than that for regular pulmonary CT angiography (CTA) examinations to allow for distribution of the contrast material in the lung parenchyma (33). Lu et al. (11) recommend bolus tracking for timing the injection with the

Main points

- Dual-energy contrast-enhanced CT can provide perfusion-based information as iodine distribution map in various pulmonary diseases, when appropriate bolus injection protocol as well as scan techniques are applied.
- Dynamic first-pass contrast-enhanced perfusion CT is able to evaluate quantitative perfusion parameters in patients with pulmonary nodule and lung cancer, and mathematical model is one of the key factors.
- Time-resolved contrast-enhanced MRA can qualitatively assess morphologic and functional information in patients with pulmonary vascular diseases.
- Dynamic contrast-enhanced perfusion MRI and quantitative perfusion indexes may be used as imaging-based biomarkers in patients with various pulmonary diseases.

detection of the region of interest in the pulmonary trunk. However, Geyer et al. (34) reported that there was no significant difference in pulmonary artery enhancement when a timing bolus was used instead of automatic bolus tracking. Patients should hold their breath at a shallow inspiratory level during scan acquisition to avoid excessive influx of unenhanced blood from the inferior vena cava, resulting from the Valsalva maneuver associated with deep inspiration. In addition, dual-energy CT scans should be acquired in the caudal-cranial direction, so that the saline chaser bolus can reach the upper chest by the time this area is acquired, to avoid streak artifacts from highly concentrated contrast media in the subclavian vein or superior vena cava. On the other hand, Nance et al. (35) reported that a protocol using a high iodine concentration and a high injection delivery rate for contrast material delivery (iomeprol 400 at 4 mL/s, corresponding to an injection delivery rate of 1.6 g I/s) resulted in the best image quality of both pulmonary multidetector row CT angiography (MDCTA) images and perfusion map images of the lung. This is due to high attenuation in the pulmonary arteries and minimization of beam-hardening artifacts compared with the protocols involving a lower concentration or lower delivery rate. Kerl et al. (36) reported that a triphasic contrast medium injection protocol (50 mL of undiluted contrast medium in the first phase, followed by a constant volume of 30 mL of a 70%:30% saline and contrast medium mixture, and 50 mL of pure saline in the third phase) could generally prevent streak artifacts from high-attenuation contrast material in the superior vena cava.

Dynamic first-pass contrast-enhanced perfusion CT

During the late 1990's and in 2000, the use of quantitatively analyzed dynamic first-pass contrast-enhanced perfusion CT by means of electron-beam CT was reported in animals and also in normal individuals and/or patients with pulmonary thromboembolism (13). However, after the introduction of multidetector row CT (MDCT) for clinical use, dynamic first-pass contrast-enhanced perfusion CT examination shifted from electron-beam CT to MDCT, and a few investigators have reported on the latter's potential for quantitative assessment of tumor or nodule perfusion assessment for diagnosis of pulmonary nodules or lung cancer, or for therapeutic effect assessment of lung cancer patients undergoing conservative therapy (14–16, 37–39). Although the number of detector rows has been increased by every vendor by 4 to 64-detector row CT systems after clinical installation of MDCT, the limited scan range attainable with dynamic scanning at the same table position or the mix of a variety of perfusion data at different time points and positions within the scan range due to the helical scan method were major drawbacks of this technique until 2007 (14–16, 37–39).

In 2007, Toshiba Medical Systems installed a 320-detector row CT system with area detector CT (ADCT) for routine clinical practice. With ADCT, isotropic volume data of lung parenchyma and nodules or masses can be acquired simultaneously within a 160 mm area without helical scan. Thus, dynamic first-pass contrast-enhanced perfusion ADCT data can be obtained by means of continuous dynamic scanning, allowing for qualitative and quantitative evaluation of perfusion of pulmonary nodules (40–42). For these reasons, ADCT systems are now being used for not only morphologic examinations, but also functional assessments, especially real first-pass evaluation of perfusion a pulmonary nodule or mass perfusion by means of the dynamic first-pass contrast-enhanced perfusion ADCT technique using mathematical models (40–42). In addition, our proprietary software developed with Toshiba causes dynamic first-pass contrast-enhanced perfusion ADCT at different table positions to generate whole-lung dynamic first-pass contrast-enhanced perfusion ADCT data, and quantitatively analyzes regional perfusion information using the mathematical models (Fig. 2). Following the introduction of Toshiba's ADCT scanner, General Electronic Healthcare also introduced a similar and new ADCT system with a 256-detector row in 2014, and has started to test its potential.

In routine clinical practice, dynamic first-pass contrast-enhanced perfusion ADCT can be performed using a dynamic volumetric scan, which can obtain 160 mm volumetric thin-section CT data without helical scan. All dynamic first-pass contrast-enhanced perfusion ADCT studies at our institution are currently performed with a 320-detector row CT scanner (40–42). Dynamic first-pass ADCT is generally obtained through the nodule within a 16.0 cm area with the following parameters: 320×0.5 mm collimation, 80kVp, 120mA, 0.5 s gantry rotation time, 512×512 matrix and 300–350 mm field of view (40–42). As contrast media injection protocol for this setting, a dual-head power injector is used for bolus administration of 20–45 mL (0.5 mL/kg body weight) of an iodinated contrast medium to all patients via a cubital vein at a rate of 5 mL/s, followed by 20 mL of saline solution at the same rate (40–42).

Although dynamic first-pass contrast-enhanced perfusion ADCT data can be obtained in routine clinical practice, it is difficult to qualitatively evaluate nodule and/or mass perfusion as well as lung parenchyma differences on dynamic first-pass contrast-enhanced perfusion ADCT images. Therefore, dynamic first-pass contrast-enhanced perfusion ADCT data for each subject is usually assessed in the form of quantitative perfusion parameter maps by means of mathematical models such as the single- and dual-input maximum slope and single-input Patlak plot models (41–43). The details of the mathematical model are not included in this paper, but several exports have suggested that the Patlak plot method is not well suited for dynamic first-pass contrast-enhanced perfusion CT data assessment for diagnosis of pulmonary nodules, nor for therapeutic effect assessment in patients with lung cancer following conservative therapy (43). Although several vendors as well as academia provide software for quantitative assessment of dynamic first-pass contrast-enhanced perfusion CT data, details of the software are usually of the black box variety. Therefore, clinicians should gain a clear understanding of the mathematical models involved in these software products before applying their clinical and academic purposes, when using dynamic first-pass contrast-enhanced perfusion CT examination in patients with pulmonary diseases.

Basics of MRI-based imaging techniques

Time-resolved contrast-enhanced MRA

Since the late 1990's, 2D or 3D contrast-enhanced MRA has been widely utilized for pulmonary vasculature assessment and perfusion evaluation in routine clinical practice. In addition, high-gradient-strength systems combined with the development of short TR 3D gradient-echo sequences made the development of single breath-hold 3D contrast-enhanced MRA possible (44–49). Depending on patients' ability to hold their breath, either high-spa-

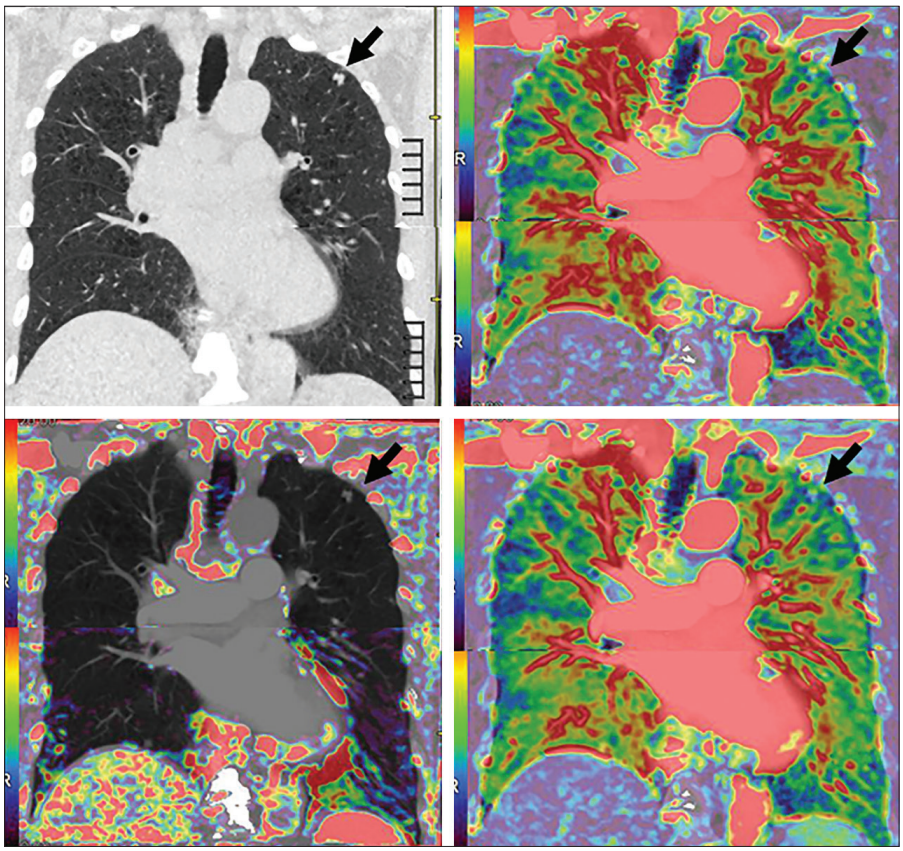

Figure 2. A 72-year-old male with pulmonary emphysema and organizing pneumonia. Left to right: thin-section multiplanar reconstructed (MPR) image and whole-lung pulmonary, systemic and total arterial perfusion maps generated from dynamic first-pass contrast-enhanced perfusion ADCT data at two different table positions analyzed by dual-input maximum slope method. Whole-lung pulmonary and total arterial perfusion maps show heterogeneously decreased perfusion due to pulmonary emphysema. In addition, organizing pneumonia *(black arrows)* is shown as low pulmonary, systemic and total arterial perfusions within the nodule.

tial resolution monophasic protocols with scan times of 20–30 s or time-resolved multiphasic imaging protocols with scan times of less than 10 s can be used (44–49). Thus, even patients with severe dyspnea can be imaged by means of time-resolved sequences.

In addition, after the introduction and clinical application of parallel imaging techniques such as sensitivity encoding (SENSE) and generalized autocalibrating partially parallel acquisitions (GRAPPA) in the early 2000's (50–52), it became possible to increase spatial and temporal resolutions of 3D contrast-enhanced MRA for not only lung, but also various other organs. Parallel imaging uses the inherent geometry of surface coils and sensitivity maps to create k-space information from under-sampled scans. Although there is a trade-off between greater speed and a reduction in signal-to-noise ratio (SNR), parallel imaging offers greater flexibility for imaging in the difficult environment of pulmonary vasculature. Since 2004, time-resolved 3D (or 4D) contrast-enhanced MRA has made it possible to increase spatial resolution to the same level as that of contrast-enhanced CTA and improve temporal resolution to less than 5 s by using 3D contrast-enhanced MRA with parallel imaging techniques for not only 1.5 Tesla (T), but also 3.0 T MRI systems (53–56). Therefore, time-resolved contrast-enhanced MRA is now considered to be one of the best MRI techniques for pulmonary vasculature and lung parenchyma perfusion evaluations of patients with various pulmonary diseases. In addition, for better visualization of pulmonary perfusion as well as better separation of pulmonary arterial, parenchymal, venous, and systemic arterial phases with this technique, time-resolved contrast-enhanced MRA should be employed with a sharp bolus injection protocol such as a total dose of 5 mL of standard-dose gadolinium contrast media with a bolus injection rate of 5 mL/s (Fig. 3) (53).

Dynamic first-pass contrast-enhanced perfusion MRI

Two general types of MRI sequences can be used to evaluate pulmonary perfusion for academic and clinical purposes: unenhanced perfusion MRI and dynamic first-pass contrast-enhanced perfusion MRI (57, 58). Although unenhanced perfusion MRI has both advantages and disadvantages compared with dynamic first-pass contrast-enhanced perfusion MRI, quantitatively and qualitatively assessed dynamic first-pass contrast-enhanced perfusion MRI has been more frequently and widely assessed due to its simpler clinical settings. This review article therefore deals with dynamic first-pass contrast-enhanced perfusion MRI in more detail.

According to these reports (19, 44, 59, 60), multiple images can be acquired during the first passage using an intravascular contrast agent through the pulmonary circulation with this technique. The images are generally obtained by using a 2D or 3D dynamic gradient-echo sequence with ultra-short echo time (TE) repetition time (TR), which are required to overcome signal loss due to the inhomogeneous magnetic susceptibility of lung tissue. Multiple images are acquired rapidly during a bolus intravenous administration of gadolinium contrast media, which also function as T1-shortening contrast agents. Images can be acquired either at multiple levels to evaluate the whole lung on 3D sequences, or at a single anatomic level on 2D sequences. In addition, images can be evaluated repeatedly during the passage of contrast material. Temporal resolution of dynamic first-pass contrast-enhanced perfusion MRI is higher than that of time-resolved contrast-enhanced MRA, and is therefore recommended for dynamic series using temporal resolution equal to or less than 1.2 s. This temporal resolution helps clinicians to clearly differentiate pulmonary arterial, parenchymal, pulmonary venous and systemic arterial phases. According to three of the reports (19, 59, 60), it also allows for quantitative assessment of pulmonary perfusion parameters similar to that performed in nuclear medicine studies as well as for dynamic first-pass contrast-enhanced ADCT by means of the principles of indicator dilution techniques. This technique provides regional pulmonary blood flow (PBF), pulmonary blood volume (PBV) and mean transit time (MTT) within the entire lung on 3D sequences and certain anatomical

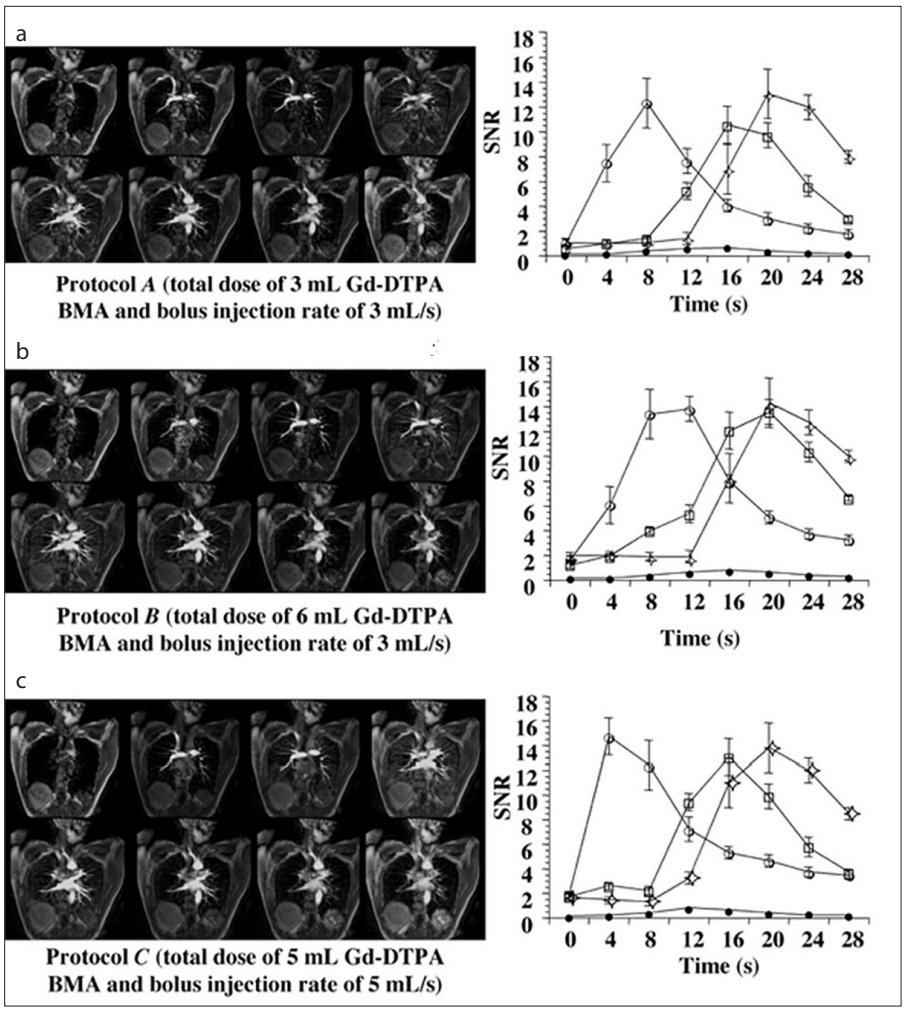

Figure 3. a–c. A 37-year-old healthy volunteer. Source images of time-resolved 3D-contrast-enhanced MRA combined with SENSE (Top row from left to right; t = 0, 4, 8, and 12 s; bottom row from left to right; t = 16, 20, and 28 s) and SNR time-course curves (empty circle, PA; solid circle, lung parenchyma; square, PV; diamond, aorta) of each bolus injection protocol. Panels **(a–c)** correspond to protocols A–C, respectively. The separation of PA and PV using protocol C was clearer than that achieved with the other protocols. SNR of the pulmonary parenchyma using protocol A was significantly lower compared with the other protocols ($P < 0.05$). In this study, all patients were administered 3 mL (protocol A) or 6 mL (protocol B) of gadodiamide (Gd-DTPA BMA) at 3 mL/s, and 5 mL of Gd-DTPA BMA at 5 mL/s (protocol C), via a cubital vein using an automatic infusion system followed by 20 mL of saline solution at the same rate for each protocol. Figure was reproduced from Ohno et al. (53) with permission.

positions within the lung on 2D sequences by means of pixel-by-pixel analysis, and clearly shows regional differences for each perfusion parameter in gravitational and iso-gravitational directions for not only normal subjects (Fig. 4), but also for patients with pulmonary diseases.

Clinical applications of imaging techniques

CT- and MRI-based perfusion assessment has been used for pulmonary diseases such as pulmonary nodules, lung cancer, chronic obstructive pulmonary diseases and pulmonary vascular diseases including pulmonary sequestration, pulmonary arterial venous fistula or malformation (PAVF or PAVM), acute or chronic pulmonary thromboembolism (PTE), and primary and secondary pulmonary arterial hypertension (PH) (17, 19, 61–66). This article focuses on the clinical applications of these techniques for pulmonary nodules, lung cancer, and pulmonary vascular diseases.

Diagnosis of pulmonary nodules

Dual-energy contrast-enhanced CT

In a study to test the utility of dual-energy CT for pulmonary nodule assessment, the detectability, number, and size of calcifications on virtual unenhanced CT images were assessed in comparison with those obtained on real unenhanced CT images. The results showed that 85% of calcifications within the nodule were detected on the virtual unenhanced CT images (30), but the calcifications seen on the virtual unenhanced CT images were smaller than those on the actual unenhanced CT images (30). This suggests that virtual unenhanced CT assessment of calcification within pulmonary nodules may not be satisfactory for the following reasons: greater image noise on the virtual than on the actual unenhanced CT images, comparatively lower SNR on the surface of calcifications, blurred edges resulting from the use of a low-pass filter, and low signal intensity of calcium removed from the iodine image during material decomposition (30). Since calcium detection within nodules implies a benign cause, the comparatively poorer depiction of calcification is one of the more serious limitations of virtual unenhanced CT.

The superior iodine distribution assessment with dual-energy CT may be even more important for routine clinical use. In contrast-enhanced CT with dual-energy CT, the material decomposition of iodine makes quantification theoretically possible by determining the CT number of pulmonary nodules on an iodine-enhanced image. Assessment of CT numbers on iodine-enhanced dual-energy CT images by subtracting the CT number on actual unenhanced CT from that on real contrast-enhanced CT images showed good agreement with the degree of enhancement determined by a conventional method. In addition, when the diagnostic performance of this technique was compared with that of traditional contrast-enhanced CT, iodine-enhanced imaging was more sensitive (23/25, 92% and accurate (37/45, 82.2%) than traditional contrast-enhancement assessment or contrast-enhanced CT (sensitivity: 18/25, 72%; accuracy: 32/45, 71.1%), whereas the specificity of the former was equal to that of the latter (14/20, 70%) (30). These results show that the iodine component is successfully decomposed from the dual-energy CT data and that virtual unenhanced CT is acceptable as a substitute for unenhanced CT. Furthermore, use of an iodine-enhanced image to measure the iodine component within a nodule can lead to a better assessment of the degree of contrast enhancement (Fig. 5). Although further investigations may be needed to determine the true clinical significance of dual-energy CT for pulmonary nodule assessment, measuring iodine values on a single scan after contrast enhancement appears to be viable

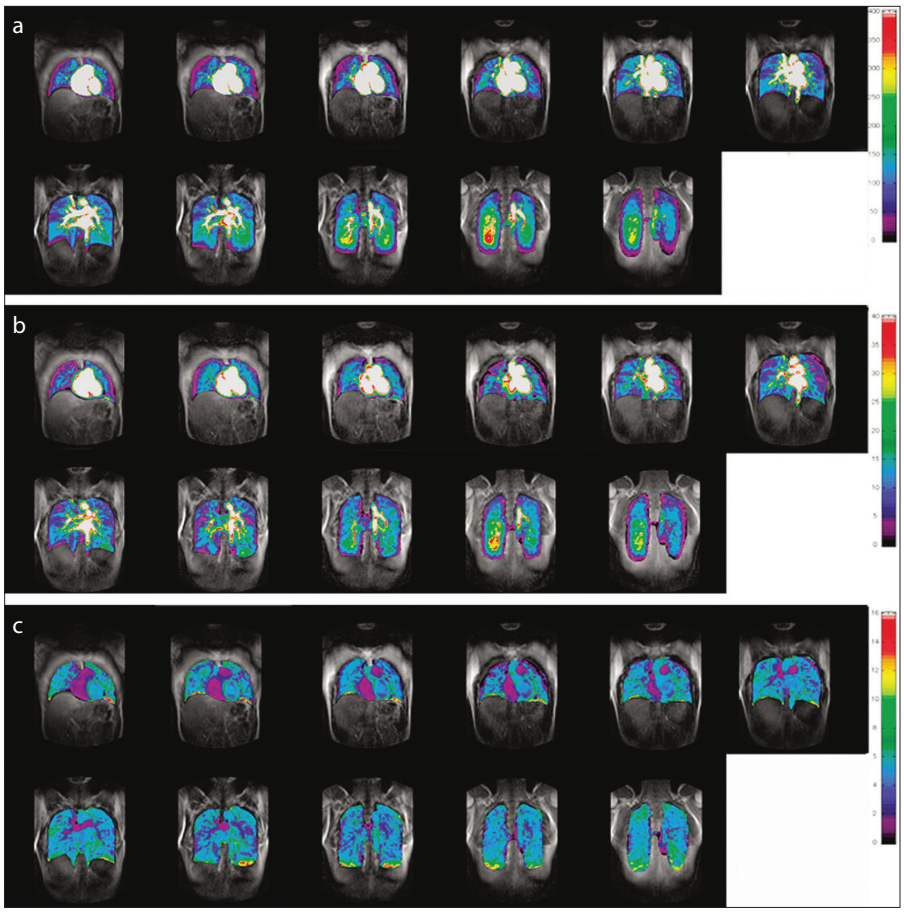

Figure 4. a–c. A 30-year-old male volunteer. Image maps **(a)** (left to right: ventral to dorsal) of pulmonary blood flow (PBF) show regional changes of PBF in the gravitational and isogravitational directions. Image maps **(b)** (left to right: ventral to dorsal) of pulmonary blood volume (PBV) demonstrate regional changes of PBV in the gravitational and isogravitational directions. Image maps **(c)** (left to right: ventral to dorsal) of mean transit time (MTT) demonstrate regional changes of MTT in the gravitational and isogravitational directions. Figure was reproduced from Ohno et al. (60) with permission.

in clinical practice, even though the iodine value does not represent the peak enhancement of the nodule.

Dynamic first-pass contrast-enhanced perfusion CT

The utility of dynamic contrast-enhanced CTs with a single-detector or MDCT scanner for differentiating malignant from benign nodules and tumors has been studied for the last few decades, and their respective sensitivities, specificities, and accuracies have been reported as 93%–100%, 52%–93%, and 77%–97% (17). Although several investigators have tested the capability of dynamic contrast-enhanced CT, one study assessed the utility of dynamic first-pass contrast-enhanced perfusion CT using 64-MDCT and the slope method as nodule perfusion analysis for differentiation of malignant from benign nodules, and reported that the sensitivity, specificity, and accuracy were 91%–94%, 82%–86%, and 90%–93%, respectively (17).

After clinical installation of ADCT in 2007, dynamic first-pass contrast-enhanced perfusion ADCT with mathematical models has been evaluated by investigators, who assessed the sensitivity, specificity, and accuracy as 65%–98%, 26%–82%, and 65%–90%, respectively (40–42). In addition, studies have directly compared the diagnostic performance of quantitatively assessed dynamic first-pass contrast-enhanced perfusion ADCT with that of PET combined with CT (PET/CT) using 2-[fluorine-18]-fluoro-2-deoxy-D-glucose (FDG) and/or dynamic first-pass contrast-enhanced MRI with ultra-short TE (40–42), and found that the diagnostic performance of dynamic first-pass contrast-enhanced perfusion ADCT for distinguishing malignant from benign nodules was equal to or better than that of the other two systems (Fig. 6). Moreover, it may be even more important to differentiate pulmonary nodules requiring further intervention and treatment (malignant nodules and benign nodules with high biologic activity) from pulmonary nodules requiring no further evaluation (benign nodules with low biologic activity) than to differentiate malignant nodules from other nodules. For this type of differentiation, quantitatively assessed dynamic first-pass contrast-enhanced ADCT has been found to be more specific and accurate for dividing all nodules into two categories (40–42). This means that quantitatively assessed dynamic first-pass contrast-enhanced ADCT should perhaps be used in routine clinical practice in a complementary role or as a substitute for dynamic contrast-enhanced CT, dynamic contrast-enhanced MRI, FDG-PET, or PET/CT to determine whether further intervention and treatment are indicated rather than to differentiate pulmonary nodules as malignant vs. benign.

Dynamic first-pass contrast-enhanced perfusion MRI

Several groups of investigators have tested dynamic contrast-enhanced MRI for its utility in differentiating malignant from benign nodules in both small and large patient populations. The findings of a meta-analysis indicated that there were no significant differences in diagnostic performance between dynamic contrast-enhanced CT, dynamic contrast-enhanced MRI with various sequences, FDG-PET, and ^{99m}Tc-depreotide SPECT (66). Therefore, dynamic contrast-enhanced MRI can be considered at least as effective as other modalities. However, a study directly comparing the diagnostic performance of semiquantitatively analyzed dynamic contrast-enhanced MRI with ultrashort TE with that of dynamic contrast-enhanced CT or PET/CT, also suggested the former's specificity and accuracy were superior to those reported for dynamic CT and almost equal to or superior to those of FDG-PET or PET/CT (67) (Fig. 7). Therefore, dynamic first-pass contrast-enhanced perfusion MRI should perhaps be used in a complementary role or as a substitute for dynamic contrast-enhanced CT and FDG-PET or PET/CT for diagnosis of pulmonary nodules in routine clinical practice.

Therapeutic effect assessment and prediction for non-small cell lung cancer

Dual-energy CT

After dual-energy CT had been clinically installed, one study found a moderate correlation between the maximum standardized uptake value (SUV_{max}) from FDG-PET/

CT and maximum iodine-related attenuation of dual-energy CT in lung cancers (68). Analyses of histologic subtypes of lung cancer showed a stronger correlation between SUV_{max} and maximum iodine-related attenuation in non-small cell lung cancer (NSCLC) than in small cell lung cancer (SCLC) (68). This difference could be explained by differences in tumor biology such as those in angiogenetic features between NSCLC and SCLC. Therefore, measurements of the maximum iodine-related attenuation on dual-energy CT may be a useful surrogate parameter for the evaluation of therapy response of lung cancer. However, a lower correlation between SUV_{max} and the maximum iodine-related attenuation in thoracic lymph nodes was noted, possibly because of differences in neo-angiogenesis between intrapulmonary tumors and lymph node metastases (68).

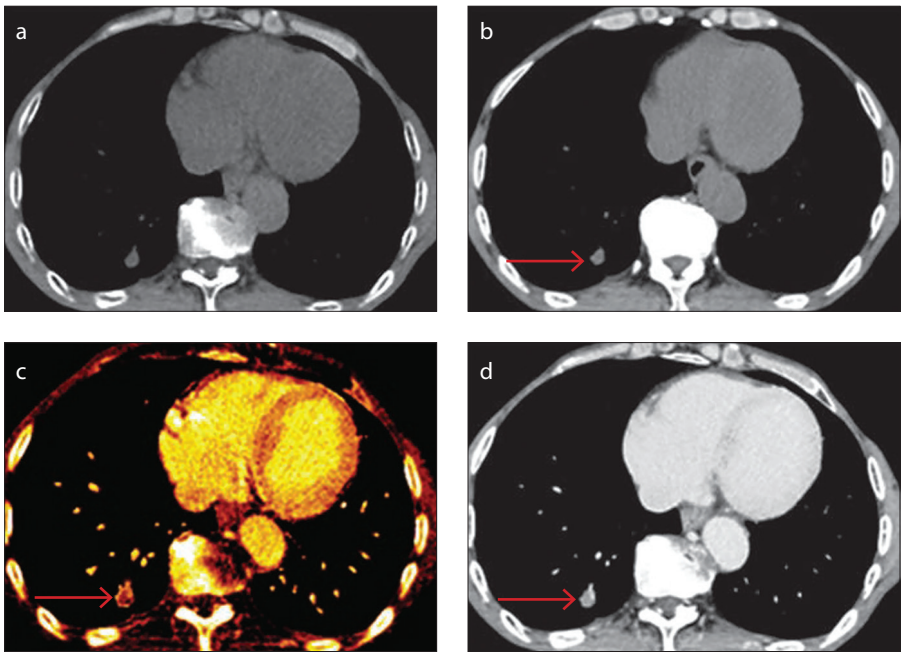

Figure 5. a–d. A 76-year-old male with metastatic lung tumor in right lower lobe (*arrows*). Virtual unenhanced CT image **(a)** obtained from contrast-enhanced CT data is well matched with unenhanced CT image **(b)** and has similar image quality. Iodine map **(c)** generated from contrast-enhanced CT data depicts iodine distribution within nodule more clearly than contrast-enhanced CT image **(d)** generated from contrast-enhanced CT data obtained at 80 and 140 kVp does. Figure was reproduced from Ohno et al. (17) with permission.

In addition, dual-phase dual-energy CT was introduced as a new tool for therapeutic effect assessment after conservative therapy including anti-angiogenesis therapy for not only primary lesions, but also mediastinal lymph node metastases in NSCLC patients (69, 70). These studies found that dual-phase dual-energy CT with iodine uptake quantification in terms of iodine uptake as well as arterial enhancement fraction is a feasible method with potential benefits for therapeutic effect prediction and/or assessment for NSCLC patients treated with conservative therapy (69, 70). In addition, this technique has the potential

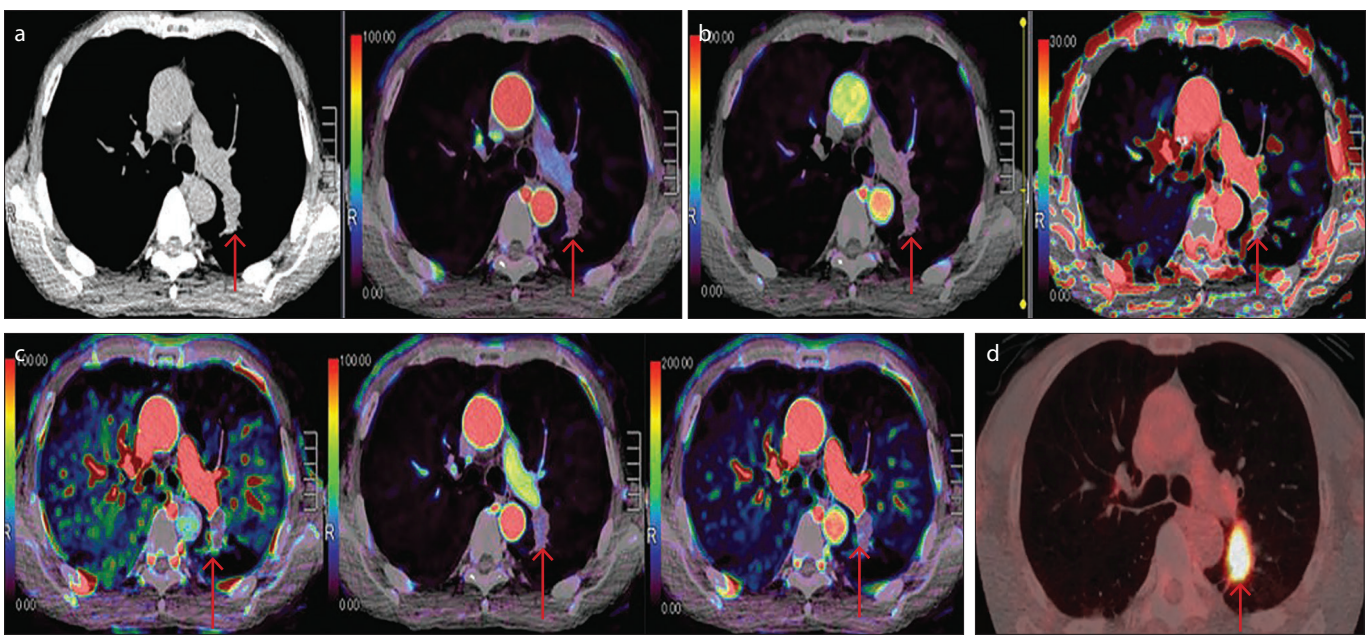

Figure 6. a–d. A 72-year-old male with invasive adenocarcinoma in left lower lobe (*arrows*). Panel **(a)** shows dynamic first-pass contrast-enhanced perfusion CT data analyzed with single-input maximum slope method. Thin-section CT image (mediastinal window setting, left) shows a nodule with invasion of left hilum. Perfusion map (right) shows low perfusion of 23 mL/100 mL/min within the nodule. Extraction fraction (left) and blood volume (right) maps **(b)** from the same data as in panel **(a)** analyzed by Patlak plot method, indicating low extraction fraction (20 mL/100 mL/min) within the nodule (left) but high distribution volume (28 mL/100 mL) (right). Pulmonary perfusion (left), systemic perfusion (center), and total perfusion (right) maps **(c)** from the same data as in panel **(a)**. Pulmonary and total perfusion maps show nodule perfusion is markedly lower than pulmonary parenchymal perfusion. Systemic perfusion map also shows low perfusion within the nodule. Pulmonary perfusion, systemic, and total nodule perfusions were calculated as 27, 23, and 50 mL/100 mL/min. FDG PET/CT image **(d)** shows high uptake of FDG within the nodule. Maximum standardized uptake value is 3.8. Figure was reproduced from Ohno et al. (17) with permission.

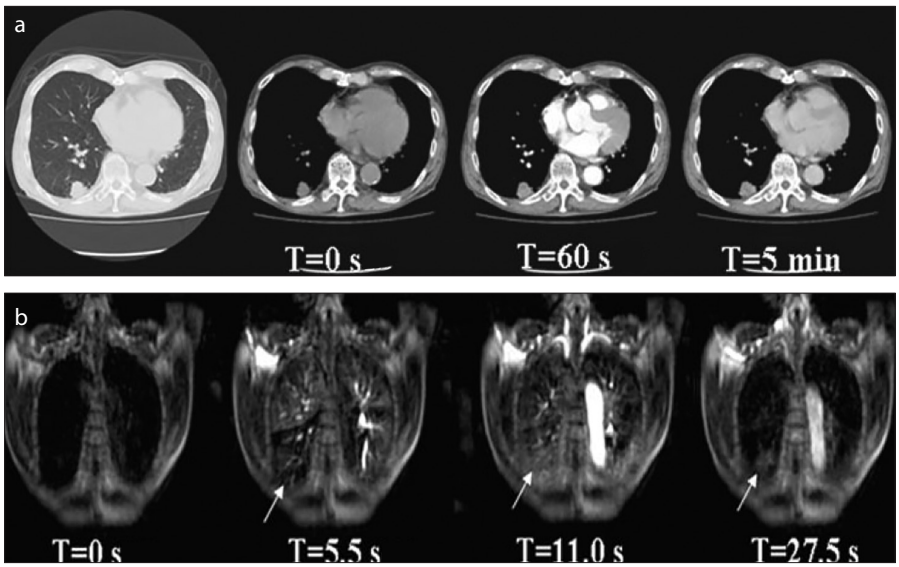

Figure 7. a–c. A 79-year-old male with adenocarcinoma of lung. Routine unenhanced (left) and dynamic contrast-enhanced CT (right) images **(a)** show a nodule with a diameter of 25 mm in the right lower lobe (T indicates time after bolus injection of contrast medium). Maximum enhancement, 73.2 HU; net enhancement, 32.4 HU; slope of enhancement, 0.54 HU/s; absolute loss of enhancement, 10.7 HU. Findings are true-positive. Dynamic contrast-enhanced MRI images **(b)** show enhancement of the nodule *(arrow)*. Maximum relative enhancement ratio is 0.36, and slope of enhancement ratio is 0.065/s. Both dynamic MRI indexes show true-positive findings. Coregistered PET/CT image **(c)** shows high uptake of FDG. Maximum standardized uptake value of lesion is 3.8. Findings are true-positive. Figure was reproduced from Ohno et al. (67) with permission.

to identify a reduction in vascularization in the responding primary lesions or metastatic lymph nodes as well as nonsignificant variable development of vascularization in nonresponding lesions (69, 70).

Dynamic first-pass contrast-enhanced perfusion CT

The standard evaluation of treatment response in the oncologic field is based on the response evaluation criteria for solid tumors, which depend on the size of tumors observed on CT (71, 72). Currently, therapeutic effect assessment and prediction may help physicians and patients to consider treatment options for personalized medicine, and have the potential to improve quality of life during and after treatment for NSCLC patients. During the past decade, several investigators have recommended two dynamic imaging techniques, dynamic first-pass contrast-enhanced perfusion MDCT and dynamic first-pass contrast-enhanced MRI using the dynamic contrast-enhanced perfusion MRI method, as equally effective for treatment response assessment during or after chemotherapy, chemoradiotherapy and/or radiotherapy procedures such as FDG-PET or PET/CT (38, 73–79). The results reported by these investigators suggest that tumor perfusion parameters can function as imaging-based biomarkers as effectively as glucose metabolism evaluated by PET or PET/CT with FDG (38, 73–79). In addition, quantitatively analyzed dynamic first-pass perfusion MDCT is a potential therapeutic effect assessment procedure based on information about angiogenetic status change for not only chemo- or chemoradiotherapy, but also antiangiogenetic therapy (38, 76–79). However, for these studies, MDCTs with a range of 4–64 detector rows were used with helical scanning employing various beam pitches and several software with mathematical models that have not been fully detailed because different versions were provided by different vendors (38, 76–79).

Since 2011, dynamic first-pass pulmonary contrast-enhanced perfusion ADCT has been in clinical use to obtain isotropic volume data within a 160 mm area without helical scan (40–42), and one study has tested its potential for quantitative therapeutic effect assessment of dynamic first-pass contrast-enhanced perfusion ADCT examination with high spatial resolution (43). Moreover, this study has suggested that, when dynamic contrast-enhanced perfusion ADCT is used, mathematical models can perform a key function in the improvement of prediction performance of therapeutic effect on NSCLC patients (43). Although further investigations are required, this technique, using the dynamic first-pass contrast-enhanced perfusion MRI method, promises to be as effective a tool for therapeutic effect assessment or prediction NSCLC patients as is FDG-PET, PET/CT, or dynamic contrast-enhanced MRI.

Dynamic first-pass contrast-enhanced perfusion MRI with ultrashort TE

Several studies have suggested that contrast-enhanced T1-weighted MRI and dynamic contrast-enhanced MRI including the perfusion MRI technique are as effective as FDG-PET or PET/CT for predicting as well as evaluating treatment response prediction or evaluation for thoracic oncology patients (17, 80). Another study has found that semiquantitatively assessed dynamic contrast-enhanced MRI using dynamic first-pass contrast-enhanced perfusion MRI can distinguish recurrence from nonrecurrence groups with a sensitivity of 55%–91%, specificity of 91%, and accuracy of 84%–91% (74). Therefore, these promising findings for the use of dynamic contrast-enhanced MRI parameters indicate that these techniques can provide additional information based on biologic changes in the behavior of tumors in NSCLC patients treated with conservative therapy. Therefore, standardization of MRI sequences, image processing, and semiquantitative or quantitative analyses are needed to realize the real significance of these techniques in this setting, which may also be used for establishing more accurate response criteria in the not too distant future.

Pulmonary thromboembolism

Dual-energy CT

Conventional pulmonary MDCT angiography can provide only morphologic information for patients with acute and

chronic PTE, but not directly assess lung parenchymal perfusion abnormalities due to thromboembolic clots. On the other hand, it has been suggested that time-resolved contrast-enhanced MRA as well as dynamic first-pass contrast-enhanced perfusion MRI can assess the latter aspect, which is important because of its implications for patient management, risk stratification, and prognostication (13, 19, 61, 62). Therefore, pulmonary MDCTA combined with an iodine distribution map on dual-energy CT is considered as more useful than conventional MDCTA because it is able to simultaneously provide pulmonary vasculature as well as lung perfusion-based information, and can evaluate functional information as a "one-stop shop" examination of patients with PTE.

Dual-energy CT for patients with PTE shows perfusion defects that are consistent with both acute and chronic PTE including those that are peripherally located, wedge-shaped, and segmentally or lobarly distributed. All other perfusion defects, such as patchy or band-like defects without segmental distribution or complete loss of color-coding are ordinarily considered inconsistent with PTE. However, several investigators have suggested that pulmonary MDCTA and dual-energy CT-based perfusion imaging may help detect lung perfusion deficits that do not have an evident morphologic thromboembolic surrogate on conventional pulmonary MDCTA (13, 81–85). Their studies reported that sensitivity and specificity on dual-energy CT on a per-segment basis were 60%–89% and 92%–100%, respectively. In addition, the corresponding values on a per-patient basis were reported by the same studies as 75%–100% and 80%–100% (13, 81–85). Moreover, it was found that dual-energy CT-based perfusion imaging increases sensitivity for the detection of PTEs, particularly for small peripheral PTEs (83). It can therefore be presumed that a simultaneous detection of a clot in a pulmonary artery on pulmonary MDCTA and of a corresponding perfusion defect on dual-energy CT-based perfusion imaging indicates occlusive PTE (13, 81–85). Pulmonary MDCTA and dual-energy CT-based perfusion imaging techniques have therefore been recommended as complementary procedures for the diagnosis of PTE in routine clinical practice.

In addition, Miura et al. (86) examined and reported that dual-energy CT may be more effective than the right ventricle/left ventricle (RV/LV) diameter ratio for disease severity assessment of patients with and without right heart dysfunction due to acute PTE. They found that the overall perfusion index, which was determined by placing the region of interest over the entire lung on a normalized lung perfused blood volume (nLung PBV) map, which was an iodine distribution map generated with commercially available software from Siemens Healthcare, was one of the predictors similar to RV/LV ratio (86). Therefore, when dual-energy CT is used for patients with suspected acute PTE, it was found that in the clinical setting it could not only diagnose acute PTE, but also more easily differentiate acute PTE patients with from those without right heart dysfunction (86). Therefore, dual-energy CT-based information may become one of the biomarkers for patients with acute PTE in routine clinical practice.

Time-resolved contrast-enhanced MRA

During the past decade, time-resolved contrast-enhanced MRA as well as contrast-enhanced MRA have been proposed as a new tool for diagnosis and patient management of PTE patients (19, 61, 62). Several studies (54, 55, 87–91) have evaluated the diagnostic performance of both non-time-resolved and time-resolved contrast-enhanced MRA for diagnosis of PTE (Table). In these studies, diagnostic performances of non-time-resolved and time-resolved contrast-enhanced MRA were evaluated as standard pulmonary digital subtraction angiography (DSA) and/or contrast-enhanced MDCT angiography, and their sensitivity and specificity were determined as 75%–100% and 95%–100%, respectively.

Another study demonstrated that the sensitivity of time-resolved contrast-enhanced MRA (83%) was significantly higher than that of contrast-enhanced MDCT angiography (75%, $P < 0.05$) on a per-vascular-zone basis, and specificity and accuracy of time-resolved contrast-enhanced MRA (specificity, 94%; accuracy, 94%) were significantly higher than those of ventilation-perfusion scan (specificity, 78% $P < 0.05$; accuracy, 75% $P < 0.05$) (54). Therefore, time-resolved contrast-enhanced MRA was found to be useful for the diagnosis of pulmonary embolism, and this technique may offer an alternative to ventilation-perfusion scintigraphy for imaging patients with suspected PTE (54).

The Prospective Investigation of Pulmonary Embolism Diagnosis III (PIOPED III) study (90), performed from 2006 to 2008, included 371 adults at seven centers, and the reference standard for this trial was determined by various tests including contrast-enhanced MDCTA and a nuclear medicine study. This study found that contrast-enhanced MRA often resulted in technically inadequate images, while the rate of such images varied considerably among centers. It was therefore concluded that the use of pulmonary contrast-enhanced MRA should be considered only at centers that routinely perform it well and only for patients for whom standard tests are contraindicated.

Dynamic first-pass contrast-enhanced perfusion MRI

Although the spatial resolution of dynamic first-pass contrast-enhanced perfusion MRI is inferior to that of time-resolved contrast-enhanced MRA, it may be more sensitive for the detection of subsegmental PTE (55, 91). Although the feeding blood vessels cannot be directly visualized, the visualization of characteristic wedge-shaped parenchymal perfusion defects allows for an indirect diagnosis of subsegmental pulmonary artery obstruction. This was also demonstrated in a recent study, where dynamic contrast-enhanced pulmonary perfusion MRI showed the highest sensitivity for assessment of PTE compared with real-time MRI with the True FISP sequence and time-resolved contrast-enhanced MRA (55, 91). In clinical practice, however, pulmonary perfusion MRI and time-resolved contrast-enhanced MRA will usually be performed as a combined protocol. Moreover, a combined protocol of dynamic contrast-enhanced perfusion MRI and time-resolved contrast-enhanced MRA showed a sensitivity and specificity for the detection of PE of over 90%, which is nearly the same as what can be attained with contrast-enhanced CTA (91).

Another study assessed the predictive value of quantitatively assessed dynamic first-pass contrast-enhanced perfusion MRI for the assessment of patient outcome for acute PTE (92). In this study, the acute PTE (APTE) index, which was defined as the ratio between the volume of perfusion defects and the total lung volume determined by means of dynamic first-pass contrast-enhanced perfusion MRI, showed accuracy for the prediction of patient outcome sim-

Table. Summary of relevant studies for assessing diagnostic performance of non-time-resolved and time-resolved contrast-enhanced MRA in patients with pulmonary thromboembolism

References	No. of patients	Methods	Gold standard	Sensitivity (%)	Specificity (%)
Meaney et al. (90)	30	3D contrast-enhanced MRA	Pulmonary DSA	75–100	95–100
Gupta et al. (91)	36	3D contrast-enhanced MRA	Pulmonary DSA	85	96
Oudkerk et al. (92)	141	3D contrast-enhanced MRA	Pulmonary DSA	77	98
Ohno et al. (54)	48	Time-resolved contrast-enhanced MRA	Pulmonary DSA	92	94
Kluge et al. (55)	62	Real-time MRI with True FISP, time-resolved contrast-enhanced MRA and dynamic contrast-enhanced perfusion MRI	16-detector row CT angiography	81	100
Stein et al. (93)	371	3D Contrast-enhanced MRA	Combination of various tests	78	99

3D, three dimensional; MRA, magnetic resonance angiography; DSA, digital subtraction angiography; MRI, magnetic resonance imaging; True FISP, true fast imaging with steady-state precession sequence; CT, computed tomography.

ilar to that of the well-investigated RV/LV diameter ratio (92). In addition, the specificity and accuracy of RV/LV diameter ratio and the APTE index determined by means of dynamic first-pass contrast-enhanced perfusion MRI were significantly higher than those of APTE indexes obtained from embolic burdens and observed on contrast-enhanced MDCTA and contrast-enhanced MRA, although logistic regression analysis demonstrated that each index was a significant predictor (92).

Pulmonary hypertension

Dual-energy CT

Since 2007 dual-energy CT has been used for not only imaging of pulmonary vascular abnormality, but also of lung parenchyma perfusion abnormalities as a single examination (13, 81, 93). It is well known that dual-energy CT has the capability to display pulmonary perfusion defects with results that are in good agreement with those obtained with perfusion scintigraphy with and without SPECT or SPECT fused with CT (SPECT/CT) (13, 81, 94, 95). Therefore, dual-energy CT is currently being intensively tested to determine its utility for patients with pulmonary hypertension including chronic thromboembolic pulmonary hypertension (CTEPH) (13, 96).

The presence and significance of perfusion abnormalities in patients with pulmonary hypertension have been most widely evaluated for patients with CTEPH (94, 97–100). The presence of consequent perfusion heterogeneity was first detected with perfusion scintigraphy (101), and more recently observed on time-resolved MRA and/or dynamic first-pass contrast-enhanced perfusion MRI (102). After installation of dual-energy CT in routine clinical practice, clinicians have been able to effectively identify this perfusion abnormality on iodine maps derived from dual-energy CT data. Furthermore, a meta-analysis reported on the capability of contrast-enhanced CTA with and without dual-energy CT or electrocardiogram-gated ADCT information for CTEPH patients (103). In this study, the patient-based analysis demonstrated a pooled sensitivity of 76%, a pooled specificity of 96%, and a pooled diagnostic odds ratio of 191. In addition, the vessel-based analyses at three different levels showed a pooled sensitivity of 88%–95%, a pooled specificity of 89%–96%, and a pooled diagnostic odds ratio of 76–751. The authors therefore concluded that CT is a suitable method for imaging proximal branches in order to differentiate between CTEPH and pulmonary endarterectomy patients. In addition, this study found that dual-energy and electrocardiogram-gated ADCT can increase the sensitivity for subsegmental arterials, thus making them promising imaging techniques for balloon pulmonary angioplasty. Further investigations are thus warranted to determine the clinical relevance of dual-energy CT for patients with CTEPH.

Time-resolved contrast-enhanced MRA and dynamic first-pass contrast-enhanced perfusion MRI

Time-resolved contrast-enhanced MRA as well as contrast-enhanced MRA have been tested as qualitative methods for patients with pulmonary hypertension due to not only CTEPH, but also other causes, while dynamic first-pass contrast-enhanced perfusion MRI has been evaluated during the past decade as a new and more sophisticated quantitative method (63, 64, 102–107) (Fig. 8). In addition, quantitatively assessed dynamic first-pass contrast-enhanced perfusion MRI has been tested to determine its utility as an imaging-based biomarker for various clinical purposes regarding patients with pulmonary hypertension (102).

Several studies have contributed to the evolution of the role of qualitative methods using time-resolved contrast-enhanced MRA as well as dynamic first-pass contrast-enhanced perfusion MRI in the workup of CTEPH (63, 64, 103–107). One of the studies found that using contrast-enhanced MDCTA as the gold standard, combined unenhanced MRI using the steady-state free precession (SSFP) sequence, contrast-enhanced MRA and contrast-enhanced perfusion MRI can improve the diagnostic performance of CTEPH as compared with contrast-enhanced MRA alone (106). In this study, the authors found that the SSFP sequence was useful for visualization of the centrally based disease of chronic clot in the main pulmonary arteries. Moreover, both contrast-enhanced MRI techniques were considered useful for the detection of disease with greater frequency compared with CTA for stenosis, post-stenotic dilation, and occlusions, although these areas of better performance could not be confirmed when the statistical method was used that assumes contrast-enhanced MDCTA as the gold standard (106). It was therefore concluded that qualitatively assessed contrast-enhanced MRA as well as dynamic first-pass contrast-enhanced perfusion MRI would appear to perform less satisfactorily than contrast-enhanced MDCTA from the point of view of simple sensitivity and specificity.

In contrast to qualitative assessments such as time-resolved contrast-enhanced MRA, contrast-enhanced MRA and dynamic

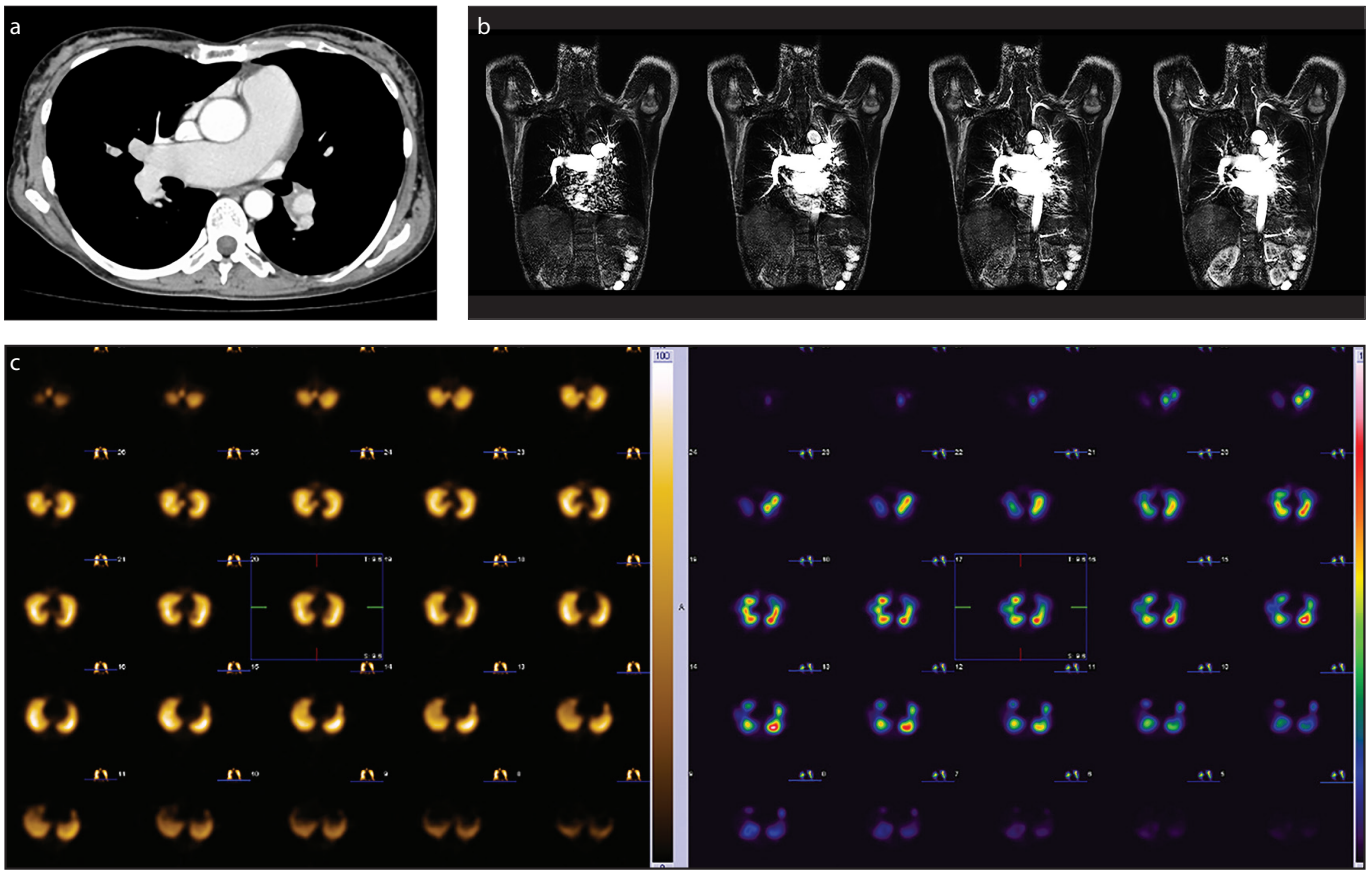

Figure 8. a–c. A 67-year-old male with chronic thromboembolic pulmonary hypertension (CTEPH). Contrast-enhanced MDCT angiography **(a)** demonstrates dilatation of pulmonary artery due to CTEPH, although no thrombi are observed. Time-resolved contrast-enhanced MRA **(b)** shows heterogeneously decreased pulmonary perfusions with no depiction of thrombi in central and peripheral pulmonary arteries. Ventilation and perfusion SPECT **(c)** demonstrate no ventilation defects and heterogeneous perfusion defect in both lungs.

first-pass contrast-enhanced perfusion MRI, quantitatively assessed 3D dynamic first-pass contrast-enhanced perfusion MRI has been continuously tested since 2004 (60). By using indicator dilution theory as well as deconvolution analysis, this method can provide quantitatively analyzed PBF, PBV and MTT information for patients with pulmonary hypertension from various causes.

The therapeutic effect of dynamic first-pass contrast-enhanced perfusion MRI on CTEPH patients was assessed for a direct comparison with contrast-enhanced MDCTA and time-resolved contrast-enhanced MRA (Fig. 9) (102). In this study, differences in pre- and post-treatment PBF, PBV and MTT showed significant correlation with improvement of patients' outcome determined by right heart catheterization and physiologic tests. In addition, application of the feasible threshold value for each index resulted in a significantly higher specificity (91%) and accuracy (96%) for the determination of improvement in PBF than for that of assessment of improvement of disease severity by means of contrast-enhanced MDCTA (specificity: 36%, $P = 0.03$; accuracy: 71%; $P = 0.03$). It can therefore be concluded that the capability of quantitatively assessed dynamic first-pass contrast-enhanced perfusion MRI for assessment of therapeutic effect on CTEPH patients is as good as or better than that of contrast-enhanced MDCTA or time-resolved contrast-enhanced MRA, and can be considered at least as effective as contrast-enhanced MDCTA and time-resolved contrast-enhanced MRA.

On the other hand, one study reported that mean regional PBF and MTT of primary pulmonary hypertension (PPH) patients were significantly different from those of healthy volunteers (108). In addition, PBF showed good negative correlation with pulmonary vascular resistance (PVR) (r=-0.79, $P < 0.0001$) and MTT and PVR moderately positive correlation (r=0.60, $P = 0.022$). Further, PBF showed moderately negative correlation with mean pulmonary arterial pressure (MPAP) (r=-0.70, $P = 0.005$), and MTT and MPAP fairly positive correlation (r=0.54, $P = 0.048$). This indicates that 3D dynamic first-pass contrast-enhanced perfusion MRI can provide clinicians with a noninvasive assessment of disease severity as indicated by PVR and MPAP in patients with PPH.

As well as for PPH patients, this technique was also tested for a direct comparison of disease severity assessment with thin-section CT for pulmonary hypertension patients with connective tissue disease (CTD) (109). In this study, systolic pulmonary arterial pressure and mean PBF of patients without pulmonary hypertension were significantly higher than of those with pulmonary hypertension ($P < 0.05$), and MTT of the former was significantly shorter than that of the latter ($P < 0.05$) (109). In addition, thin-section CT-based disease severity showed significantly good and negative correlation with mean PBF (r=-0.77, $P < 0.01$) and mean PBV (r=-0.59, $P = 0.01$), and significantly moderate and positive correlation with MTT (r=0.65, $P < 0.01$). Therefore, quantitatively assessed

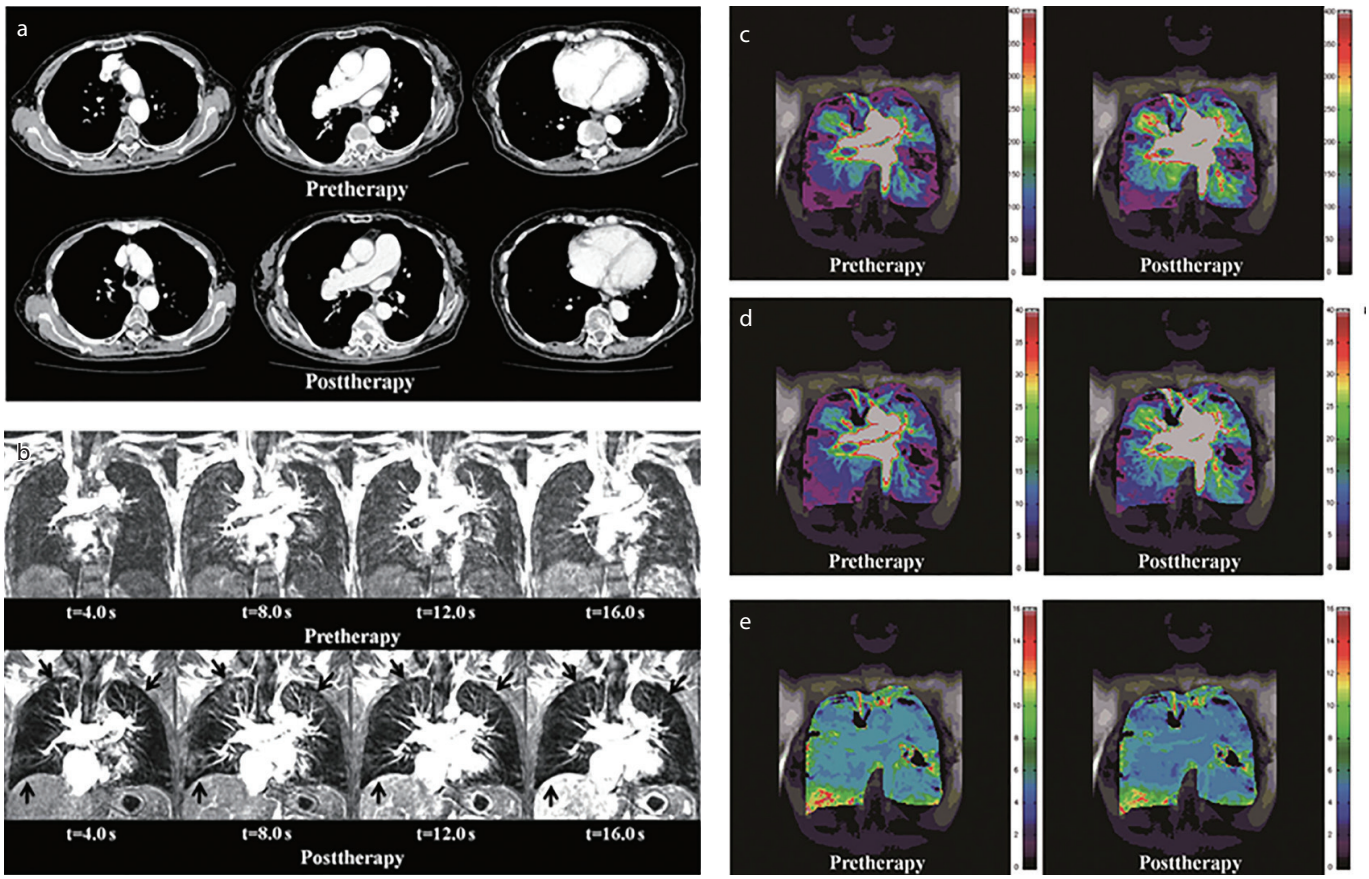

Figure 9. a–e. A 76-year-old male with CTEPH treated with conservative therapy and assessed as responder. Contrast-enhanced MDCT **(a)** (top to bottom: pretherapeutic MDCT to post-therapeutic MDCT; left to right: cranial to caudal) demonstrates presence of thrombi in subsegmental pulmonary arteries. Although some subsegmental thrombi disappeared, improvement in $CTEPH_{CTA}$ was 0%, but improvement in the RV/LV diameter ratio was -0.05. This case was identified as true positive on contrast-enhanced MDCTs. Source images of time-resolved contrast-enhanced MRA **(b)** (top to bottom: pretherapeutic time-resolved contrast-enhanced MRA to post-therapeutic time-resolved contrast-enhanced MRA; left to right: ventral to dorsal) shows pulmonary parenchymal enhancement in both lungs, while improvement in $CTEPH_{MRA}$ was -13.5%. This case was identified as true positive on time-resolved contrast-enhanced MRA. Quantitative PBF maps **(c)** (left to right: pretherapy to post-therapy) demonstrate improvement in PBF in both lungs to 57 mL/100 mL/min, respectively. This case was identified as true positive on PBF maps. Quantitative PBV maps **(d)** (left to right: pretherapy to post-therapy) demonstrate improvement in PBF in both lungs, while PBV improved by 12 mL/100 mL. This case was identified as true positive on PBV maps. Quantitative MTT maps **(e)** (left to right: pretherapy to post-therapy) demonstrate improved PBF in both lungs, while MTT improved by -2.3 s. This case was identified as true positive on MTT maps. Figure was reproduced from Ohno et al. (102) with permission.

3D dynamic first-pass contrast-enhanced perfusion MRI appears to have good potential for assessment of disease severity and progression of pulmonary hypertension in CTD patients. Moreover, this technique, similar to Doppler echocardiography and the pulmonary function test, may be useful for noninvasive physiopathologic assessment of CTD patients, and may be used as a substitute for right heart catheterization for CTD patients with pulmonary hypertension.

Although further investigations are warranted, quantitatively assessed dynamic first-pass contrast-enhanced perfusion MRI may in the near future be able to perform a complementary role in the management of patients with pulmonary hypertension from various causes in routine clinical practice.

Conclusion

New contrast-enhanced imaging techniques such as dual-energy CT, dynamic first-pass contrast-enhanced perfusion ADCT, time-resolved contrast-enhanced MRA, and dynamic first-pass contrast-enhanced perfusion MRI of the lung are useful for not only thoracic oncology patients, but also patients with various pulmonary vascular diseases in routine clinical practice. While the first-pass contrast agent technique is minimally invasive but associated with risks and high costs for contrast administration, these new techniques are simple and easily applied in the clinical setting. Moreover, some of these techniques can potentially be used for quantitative assessment of regional pulmonary perfusion, nodule or tumor parameters, and physiologic and pathophysiologic analysis of various pulmonary diseases. Future developments in image acquisition and postprocessing for quantitative analyses can enhance the clinical application of these techniques for evaluation of pulmonary diseases, as well as expand their clinical relevance to other thoracic diseases.

Acknowledgements

Authors thank Yuji Kishida, MD, Shinichiro Seki, MD PhD (Department of Radiology, Kobe University Graduate School of Medicine), Noriyuki Negi, RT, Katsusuke Kyotani, RT, Tohru Murakami, RT (Center for Radiology and Radiation Oncology, Kobe University Hospital), Yoshimasa Maniwa, MD PhD (Division of Thoracic Surgery, Department of Surgery, Kobe University Graduate School of Medicine), Yoshihiro Nishimura, MD PhD (Division of Respiratory Medicine, Department of Internal Medicine, Kobe University Graduate School of Medicine), Kenichi Hirata, MD PhD (Division of Cardiovascular Medicine, Department of Internal Medicine, Kobe University

Graduate School of Medicine), and Kimihiko Kichikawa, MD (Department of Radiology, Nara Medical University) for their contribution to this work.

Financial disclosure

This work is financially and/ or technically supported by Toshiba Medical Systems, Philips Electronics Japan, Bayer Pharma, Guerbet, Daiichi-Sankyo, Eizai, Fuji RI Pharma, and Fuji Pharma.

Conflict of interest disclosure

Drs. Ohno, Yoshikawa and Sugimura have research grants from Toshiba Medical Systems, Philips Electronics Japan, Bayer Pharma, Guerbet, Daiichi-Sankyo, Eizai, Fuji RI Pharma and Fuji Pharma.

References

1. Wagner HN Jr. The use of radioisotope techniques for the evaluation of patients with pulmonary disease. Am Rev Respir Dis 1976; 113:203–218.
2. Pistolesi M, Miniati M, Di Ricco G, Marini C, Giuntini C. Perfusion lung imaging in the adult respiratory distress syndrome. J Thorac Imaging 1986; 1:11–24. [CrossRef]
3. Schuster DP. ARDS: clinical lessons from the oleic acid model of acute lung injury. Am J Respir Crit Care Med 1994; 149:245–260. [CrossRef]
4. Schuster DP, Kaplan JD, Gauvain K, Welch MJ, Markham J. Measurement of regional pulmonary blood flow with PET. J Nucl Med 1995; 36:371–377.
5. Kawakami K. Topics in pulmonary nuclear medicine. Ann Nucl Med 1997; 11:67–73. [CrossRef]
6. Lewis DH, Kott B, Jacobson AF. Single-photon emission tomography imaging of the chest. Respir Care 2001; 46:940–945.
7. Musch G, Venegas JG. Positron emission tomography imaging of regional pulmonary perfusion and ventilation. Proc Am Thorac Soc 2005; 2:522–527. [CrossRef]
8. Petersson J, Sánchez-Crespo A, Larsson SA, Mure M. Physiological imaging of the lung: single-photon-emission computed tomography (SPECT). J Appl Physiol 2007; 102:468–476. [CrossRef]
9. Suga K. Pulmonary function-morphologic relationships assessed by SPECT-CT fusion images. Ann Nucl Med 2012; 26:298–310. [CrossRef]
10. Chae EJ, Song JW, Krauss B, et al. Dual-energy computed tomography characterization of solitary pulmonary nodules. J Thorac Imaging 2010; 25:301–310. [CrossRef]
11. Lu GM, Zhao Y, Zhang LJ, Schoepf UJ. Dual-energy CT of the lung. AJR Am J Roentgenol 2012; 199:S40–S53. [CrossRef]
12. Remy-Jardin M, Faivre JB, Pontana F, Molinari F, Tacelli N, Remy J. Thoracic applications of dual energy. Semin Respir Crit Care Med 2014; 35:64–73. [CrossRef]
13. Schoepf UJ, Bruening R, Konschitzky H, et al. Pulmonary embolism: comprehensive diagnosis by using electron-beam CT for detection of emboli and assessment of pulmonary blood flow. Radiology 2000; 217:693–700. [CrossRef]
14. Herzog P, Wildberger JE, Niethammer M, Schaller S, Schoepf UJ. CT perfusion imaging of the lung in pulmonary embolism. Acad Radiol 2003; 10:1132–1146. [CrossRef]
15. Hoffman EA, Chon D. Computed tomography studies of lung ventilation and perfusion. Proc Am Thorac Soc 2005; 2:492–498. [CrossRef]
16. Ng QS, Goh V, Fichte H, et al. Lung cancer perfusion at multi-detector row CT: reproducibility of whole tumor quantitative measurements. Radiology 2006; 239:547–553. [CrossRef]
17. Ohno Y, Nishio M, Koyama H, et al. Dynamic contrast-enhanced CT and MRI for pulmonary nodule assessment. AJR Am J Roentgenol 2014; 202:515–529. [CrossRef]
18. Uematsu H, Ohno Y, Hatabu H. Recent advances in magnetic resonance perfusion imaging of the lung. Top Magn Reson Imaging. 2003; 14: 245–251. [CrossRef]
19. Pedersen MR, Fisher MT, van Beek EJ. MR imaging of the pulmonary vasculature--an update. Eur Radiol 2006; 16:1374–1386. [CrossRef]
20. Matsuoka S, Hunsaker AR, Gill RR, et al. Functional MR imaging of the lung. Magn Reson Imaging Clin N Am 2008; 16:275–289. [CrossRef]
21. Sieren JC, Ohno Y, Koyama H, Sugimura K, McLennan G. Recent technological and application developments in computed tomography and magnetic resonance imaging for improved pulmonary nodule detection and lung cancer staging. J Magn Reson Imaging 2010; 32:1353–1369. [CrossRef]
22. Ley S, Ley-Zaporozhan J. Pulmonary perfusion imaging using MRI: clinical application. Insights Imaging 2012; 3:61–71. [CrossRef]
23. Ohno Y. New applications of magnetic resonance imaging for thoracic oncology. Semin Respir Crit Care Med 2014; 35:27–40. [CrossRef]
24. Genant HK, Boyd D. Quantitative bone mineral analysis using dual energy computed tomography. Invest Radiol 1977; 12:545–551. [CrossRef]
25. Chiro GD, Brooks RA, Kessler RM, et al. Tissue signatures with dual-energy computed tomography. Radiology 1979; 131:521–523. [CrossRef]
26. Millner MR, McDavid WD, Waggener RG, Dennis MJ, Payne WH, Sank V. Extraction of information from CT scans at different energies. Med Phys 1979; 6:70–71. [CrossRef]
27. Flohr TG, McCollough CH, Bruder H, et al. First performance evaluation of a dual-source CT (DSCT) system. Eur Radiol 2006; 16:256–268. [CrossRef]
28. Ko JP, Brandman S, Stember J, Naidich DP. Dual-energy computed tomography: concepts, performance, and thoracic applications. J Thorac Imaging 2012; 27:7–22. [CrossRef]
29. Kaza RK, Platt JF, Cohan RH, Caoili EM, Al-Hawary MM, Wasnik A. Dual-energy CT with single- and dual-source scanners: current applications in evaluating the genitourinary tract. Radiographics 2012; 32:353–369. [CrossRef]
30. Chae EJ, Song JW, Seo JB, Krauss B, Jang YM, Song KS. Clinical utility of dual-energy CT in the evaluation of solitary pulmonary nodules: initial experience. Radiology 2008; 249:671–681. [CrossRef]
31. Kang MJ, Park CM, Lee CH, Goo JM, Lee HJ. Dual-energy CT: clinical applications in various pulmonary diseases. Radiographics 2010; 30:685–698. [CrossRef]
32. Johnson TR, Krauss B, Sedlmair M, et al. Material differentiation by dual energy CT: initial experience. Eur Radiol 2007; 17:1510–1517. [CrossRef]
33. Thieme SF, Johnson TR, Lee C, et al. Dual-energy CT for the assessment of contrast material distribution in the pulmonary parenchyma. AJR Am J Roentgenol 2009; 193:144–149. [CrossRef]
34. Geyer LL, Scherr M, Körner M, et al. Imaging of acute pulmonary embolism using a dual energy CT system with rapid kVp switching: initial results. Eur J Radiol 2012; 81:3711–3718. [CrossRef]
35. Nance JW Jr, Henzler T, Meyer M, et al. Optimization of contrast material delivery for dual-energy computed tomography pulmonary angiography in patients with suspected pulmonary embolism. Invest Radiol 2012; 47:78–84. [CrossRef]
36. Kerl JM, Bauer RW, Renker M, et al. Triphasic contrast injection improves evaluation of dual energy lung perfusion in pulmonary CT angiography. Eur J Radiol 2011; 80:e483–e487. [CrossRef]
37. Sitartchouk I, Roberts HC, Pereira AM, Bayanati H, Waddell T, Roberts TP. Computed tomography perfusion using first pass methods for lung nodule characterization. Invest Radiol 2008; 43:349–358. [CrossRef]
38. Wang J, Wu N, Cham MD, Song Y. Tumor response in patients with advanced non-small cell lung cancer: perfusion CT evaluation of chemotherapy and radiation therapy. AJR Am J Roentgenol 2009; 193:1090–1096. [CrossRef]
39. Li Y, Yang ZG, Chen TW, Yu JQ, Sun JY, Chen HJ. First-pass perfusion imaging of solitary pulmonary nodules with 64-detector row CT: comparison of perfusion parameters of malignant and benign lesions. Br J Radiol 2010; 83:785–790. [CrossRef]
40. Ohno Y, Koyama H, Matsumoto K, et al. Differentiation of malignant and benign pulmonary nodules with quantitative first-pass 320-detector row perfusion CT versus FDG PET/CT. Radiology 2011; 258:599–609. [CrossRef]
41. Ohno Y, Nishio M, Koyama H, et al. Comparison of quantitatively analyzed dynamic area-detector CT using various mathematic methods with FDG PET/CT in management of solitary pulmonary nodules. AJR Am J Roentgenol 2013; 200:W593–W602. [CrossRef]
42. Ohno Y, Nishio M, Koyama H, et al. Solitary pulmonary nodules: Comparison of dynamic first-pass contrast-enhanced perfusion area-detector CT, dynamic first-pass contrast-enhanced MR imaging, and FDG PET/CT. Radiology 2015; 274:563–575. [CrossRef]
43. Ohno Y, Koyama H, Fujisawa Y, et al. Dynamic contrast-enhanced perfusion area detector ct for non-small cell lung cancer patients: influence of mathematical models on early prediction capabilities for treatment response and recurrence after chemoradiotherapy. Eur J Radiol 2016; 85:176–186. [CrossRef]
44. Hatabu H, Gaa J, Kim D, Li W, Prasad PV, Edelman RR. Pulmonary perfusion and angiography: evaluation with breath-hold enhanced three-dimensional fast imaging steady-state precession MR imaging with short TR and TE. AJR Am J Roentgenol 1996; 167:653–655. [CrossRef]
45. Leung DA, McKinnon GC, Davis CP, Pfammatter T, Krestin GP, Debatin JF. Breath-hold, contrast-enhanced, three-dimensional MR angiography. Radiology 1996; 200:569–571. [CrossRef]
46. Kauczor HU. Contrast-enhanced magnetic resonance angiography of the pulmonary vasculature. A review. Invest Radiol 1998; 33:606–617.[CrossRef]
47. Ohno Y, Adachi S, Motoyama A, et al. Multiphase ECG-triggered 3D contrast-enhanced MR angiography: utility for evaluation of hilar and mediastinal invasion of bronchogenic carcinoma. J Magn Reson Imaging 2001; 13:215–224. [CrossRef]
48. Goyen M, Ruehm SG, Jagenburg A, Barkhausen J, Kröger K, Debatin JF. Pulmonary arteriovenous malformation: Characterization with time-resolved ultrafast 3D MR angiography. J Magn Reson Imaging 2001; 13:458–460. [CrossRef]
49. Fink C, Bock M, Kiessling F, et al. Time-resolved contrast-enhanced three-dimensional pulmonary MR-angiography: 1.0 M gadobutrol vs. 0.5 M gadopentetate dimeglumine. J Magn Reson Imaging 2004; 19:202–208. [CrossRef]

50. Pruessmann KP, Weiger M, Scheidegger MB, Boesiger P. SENSE: sensitivity encoding for fast MRI. Magn Reson Med 1999; 42:952–962. [CrossRef]
51. Griswold MA, Jakob PM, Heidemann RM, et al. Generalized autocalibrating partially parallel acquisitions (GRAPPA). Magn Reson Med 2002; 47:1202–1210. [CrossRef]
52. Blaimer M, Breuer F, Mueller M, Heidemann RM, Griswold MA, Jakob PM. SMASH, SENSE, PILS, GRAPPA: how to choose the optimal method. Top Magn Reson Imaging 2004; 15:23–36. [CrossRef]
53. Ohno Y, Kawamitsu H, Higashino T, et al. Time-resolved contrast-enhanced pulmonary MR angiography using sensitivity encoding (SENSE). J Magn Reson Imaging 2003; 17:330–336. [CrossRef]
54. Ohno Y, Higashino T, Takenaka D, et al. MR angiography with sensitivity encoding (SENSE) for suspected pulmonary embolism: comparison with MDCT and ventilation-perfusion scintigraphy. AJR Am J Roentgenol 2004; 183:91–98. [CrossRef]
55. Kluge A, Luboldt W, Bachmann G. Acute pulmonary embolism to the subsegmental level: diagnostic accuracy of three MRI techniques compared with 16-MDCT. AJR Am J Roentgenol 2006; 187:W7–W14. [CrossRef]
56. Ohno Y, Nishio M, Koyama H, et al. Journal Club: Comparison of assessment of preoperative pulmonary vasculature in patients with non-small cell lung cancer by non-contrast- and 4D contrast-enhanced 3-T MR angiography and contrast-enhanced 64-MDCT. AJR Am J Roentgenol. 2014; 202:493–506. [CrossRef]
57. Hecht EM, Rosenkrantz A. Pulmonary MR angiography techniques and applications. Magn Reson Imaging Clin N Am 2009; 17:101–131. [CrossRef]
58. Miyazaki M, Akahane M. Non-contrast enhanced MR angiography: established techniques. J Magn Reson Imaging 2012; 35:1–19. [CrossRef]
59. Levin DL, Chen Q, Zhang M, Edelman RR, Hatabu H. Evaluation of regional pulmonary perfusion using ultrafast magnetic resonance imaging. Magn Reson Med 2001; 46: 166–171. [CrossRef]
60. Ohno Y, Hatabu H, Murase K, et al. Quantitative assessment of regional pulmonary perfusion in the entire lung using three-dimensional ultrafast dynamic contrast-enhanced magnetic resonance imaging: Preliminary experience in 40 subjects. J Magn Reson Imaging 2004; 20:353–365. [CrossRef]
61. Coulden R. State-of-the-art imaging techniques in chronic thromboembolic pulmonary hypertension. Proc Am Thorac Soc 2006; 3:577–583. [CrossRef]
62. Kuriakose J, Patel S. Acute pulmonary embolism. Radiol Clin North Am 2010; 48:31–50. [CrossRef]
63. Ley S, Grünig E, Kiely DG, van Beek E, Wild J. Computed tomography and magnetic resonance imaging of pulmonary hypertension: Pulmonary vessels and right ventricle. J Magn Reson Imaging 2010; 32:1313–1324. [CrossRef]
64. Kreitner KF. Noninvasive imaging of pulmonary hypertension. Semin Respir Crit Care Med 2014; 35:99–111. [CrossRef]
65. Hoffman EA, Lynch DA, Barr RG, van Beek EJ, Parraga G; IWPFI Investigators. Pulmonary CT and MRI phenotypes that help explain chronic pulmonary obstruction disease pathophysiology and outcomes. J Magn Reson Imaging 2016; 43:544–557. [CrossRef]
66. Cronin P, Dwamena BA, Kelly AM, Carlos RC. Solitary pulmonary nodules: meta-analytic comparison of cross-sectional imaging modalities for diagnosis of malignancy. Radiology 2008; 246:772–782. [CrossRef]
67. Ohno Y, Koyama H, Takenaka D, et al. Dynamic MRI, dynamic multidetector-row computed tomography (MDCT), and coregistered 2-[fluorine-18]-fluoro-2-deoxy-D-glucose-positron emission tomography (FDG-PET)/CT: comparative study of capability for management of pulmonary nodules. J Magn Reson Imaging 2008; 27:1284–1295. [CrossRef]
68. Schmid-Bindert G, Henzler T, Chu TQ, et al. Functional imaging of lung cancer using dual energy CT: how does iodine related attenuation correlate with standardized uptake value of 18FDG-PET-CT? Eur Radiol 2012; 22:93–103. [CrossRef]
69. Baxa J, Vondráková A, Matoušková T, et al. Dual-phase dual-energy CT in patients with lung cancer: assessment of the additional value of iodine quantification in lymph node therapy response. Eur Radiol 2014; 24:1981–1988. [CrossRef]
70. Baxa J, Matouskova T, Krakorova G, et al. Dual-phase dual-energy CT in patients treated with erlotinib for advanced non-small cell lung cancer: possible benefits of iodine quantification in response assessment. Eur Radiol 2015 Nov 12. [Epub ahead of print]
71. Therasse P, Arbuck SG, Eisenhauer EA, et al. New guidelines to evaluate the response to treatment in solid tumors. European Organization for Research and Treatment of Cancer, National Cancer Institute of the United States, National Cancer Institute of Canada. J Natl Cancer Inst 2000; 92:205–216. [CrossRef]
72. Eisenhauer EA, Therasse P, Bogaerts J, et al. New response evaluation criteria in solid tumours: revised RECIST guideline (version 1.1). Eur J Cancer 2009; 45:228–247. [CrossRef]
73. Mac Manus MP, Hicks RJ, Matthews JP, et al. Positron emission tomography is superior to computed tomography scanning for response-assessment after radical radiotherapy or chemoradiotherapy in patients with non-small-cell lung cancer. J Clin Oncol 2003; 21:1285–1292. [CrossRef]
74. Ohno Y, Nogami M, Higashino T, et al. Prognostic value of dynamic MR imaging for non-small-cell lung cancer patients after chemoradiotherapy. J Magn Reson Imaging 2005; 21:775–783. [CrossRef]
75. Mac Manus M, Hicks RJ, Everitt S. Role of PET-CT in the optimization of thoracic radiotherapy. J Thorac Oncol 2006; 1:81–84. [CrossRef]
76. Ng QS, Goh V, Milner J, et al. Quantitative helical dynamic contrast enhanced computed tomography assessment of the spatial variation in whole tumour blood volume with radiotherapy in lung cancer. Lung Cancer 2010; 69:71–76. [CrossRef]
77. Fraioli F, Anzidei M, Zaccagna F, et al. Whole-tumor perfusion CT in patients with advanced lung adenocarcinoma treated with conventional and antiangiogenetic chemotherapy: initial experience. Radiology 2011; 259:574–582. [CrossRef]
78. Tacelli N, Santangelo T, Scherpereel A, et al. Perfusion CT allows prediction of therapy response in non-small cell lung cancer treated with conventional and anti-angiogenic chemotherapy. Eur Radiol 2013; 23:2127–2136. [CrossRef]
79. Sudarski S, Shi J, Schmid-Bindert G, et al. Dynamic volume perfusion CT parameters versus RECIST for the prediction of outcome in lung cancer patients treated with conventional chemotherapy. J Thorac Oncol 2015; 10:164–171. [CrossRef]
80. Nishino M, Hatabu H, Johnson BE, McLoud TC. State of the art: Response assessment in lung cancer in the era of genomic medicine. Radiology 2014; 271:6–27. [CrossRef]
81. Thieme SF, Becker CR, Hacker M, Nikolaou K, Reiser MF, Johnson TR. Dual energy CT for the assessment of lung perfusion--correlation to scintigraphy. Eur J Radiol. 2008; 68:369–374. [CrossRef]
82. Pontana F, Faivre JB, Remy-Jardin M, et al. Lung perfusion with dual-energy multidetector-row CT (MDCT): feasibility for the evaluation of acute pulmonary embolism in 117 consecutive patients. Acad Radiol 2008; 15:1494–1504. [CrossRef]
83. Lu GM, Wu SY, Yeh BM, Zhang LJ. Dual-energy computed tomography in pulmonary embolism. Br J Radiol 2010; 83:707–718. [CrossRef]
84. Wu HW, Cheng JJ, Li JY, Yin Y, Hua J, Xu JR. Pulmonary embolism detection and characterization through quantitative iodine-based material decomposition images with spectral computed tomography imaging. Invest Radiol 2012; 47:85–91. [CrossRef]
85. Zhang LJ, Wang ZJ, Zhou CS, Lu L, Luo S, Lu GM. Evaluation of pulmonary embolism in pediatric patients with nephrotic syndrome with dual energy CT pulmonary angiography. Acad Radiol 2012; 19:341–348. [CrossRef]
86. Miura S, Ohno Y, Kimura H, Kichikawa K. Quantitative lung perfused blood volume imaging on dual-energy CT: capability for quantitative assessment of disease severity in patients with acute pulmonary thromboembolism. Acta Radiol 2015; 56:284–293. [CrossRef]
87. Meaney JF, Weg JG, Chenevert TL, Stafford-Johnson D, Hamilton BH, Prince MR. Diagnosis of pulmonary embolism with magnetic resonance angiography. N Engl J Med 1997; 336:1422–1427. [CrossRef]
88. Gupta A, Frazer CK, Ferguson JM, et al. Acute pulmonary embolism: diagnosis with MR angiography. Radiology 1999; 210:353–359. [CrossRef]
89. Oudkerk M, van Beek EJ, Wielopolski P, et al. Comparison of contrast-enhanced magnetic resonance angiography and conventional pulmonary angiography for the diagnosis of pulmonary embolism: a prospective study. Lancet 2002; 359:1643–1647. [CrossRef]
90. Stein PD, Chenevert TL, Fowler SE, et al; PIOPED III (Prospective Investigation of Pulmonary Embolism Diagnosis III) Investigators. Gadolinium-enhanced magnetic resonance angiography for pulmonary embolism: a multicenter prospective study (PIOPED III). Ann Intern Med 2010; 152:434–443. [CrossRef]
91. Kluge A, Mueller C, Strunk J, Lange U, Bachmann G. Experience in 207 combined MRI examinations for acute pulmonary embolism and deep vein thrombosis. AJR Am J Roentgenol 2006; 186:1686–1696. [CrossRef]
92. Ohno Y, Koyama H, Matsumoto K, et al. Dynamic MR perfusion imaging: capability for quantitative assessment of disease extent and prediction of outcome for patients with acute pulmonary thromboembolism. J Magn Reson Imaging 2010; 31:1081–1090. [CrossRef]
93. Remy-Jardin M, Pistolesi M, Goodman LR, et al. Management of suspected acute pulmonary embolism in the era of CT angiography: a statement from the Fleischner Society. Radiology 2007; 245:315–329. [CrossRef]

94. Nakazawa T, Watanabe Y, Hori Y, et al. Lung perfused blood volume images with dual-energy computed tomography for chronic thromboembolic pulmonary hypertension: correlation to scintigraphy with single-photon emission computed tomography. J Comput Assist Tomogr 2011; 35:590–595. [CrossRef]
95. Thieme SF, Graute V, Nikolaou K, et al. Dual Energy CT lung perfusion imaging--correlation with SPECT/CT. Eur J Radiol 2012; 81:360–365. [CrossRef]
96. Junqueira FP, Lima CM, Coutinho AC Jr, et al. Pulmonary arterial hypertension: an imaging review comparing MR pulmonary angiography and perfusion with multidetector CT angiography. Br J Radiol 2012; 85:1446–1456. [CrossRef]
97. Hoey ET, Agrawal SK, Ganesh V, Gopalan D, Screaton NJ. Dual energy CT pulmonary angiography: findings in a patient with chronic thromboembolic pulmonary hypertension. Thorax 2009; 64:1012. [CrossRef]
98. Hoey ET, Mirsadraee S, Pepke-Zaba J, Jenkins DP, Gopalan D, Screaton NJ. Dual-energy CT angiography for assessment of regional pulmonary perfusion in patients with chronic thromboembolic pulmonary hypertension: initial experience. AJR Am J Roentgenol 2011; 196:524–532. [CrossRef]
99. Renard B, Remy-Jardin M, Santangelo T, et al. Dual-energy CT angiography of chronic thromboembolic disease: can it help recognize links between the severity of pulmonary arterial obstruction and perfusion defects? Eur J Radiol 2011; 79:467–472. [CrossRef]
100. Soler X, Kerr KM, Marsh JJ, et al. Pilot study comparing SPECT perfusion scintigraphy with CT pulmonary angiography in chronic thromboembolic pulmonary hypertension. Respirology 2012; 17:180–184. [CrossRef]
101. Lisbona R, Kreisman H, Novales-Diaz J, Derbekyan V. Perfusion lung scanning: differentiation of primary from thromboembolic pulmonary hypertension. AJR Am J Roentgenol 1985; 144:27–30. [CrossRef]
102. Ohno Y, Koyama H, Yoshikawa T, et al. Contrast-enhanced multidetector-row computed tomography vs. Time-resolved magnetic resonance angiography vs. contrast-enhanced perfusion MRI: assessment of treatment response by patients with inoperable chronic thromboembolic pulmonary hypertension. J Magn Reson Imaging 2012; 36:612–623. [CrossRef]
103. Dong C, Zhou M, Liu D, Long X, Guo T, Kong X. Diagnostic accuracy of computed tomography for chronic thromboembolic pulmonary hypertension: a systematic review and meta-analysis. PLoS One 2015; 10:e0126985. [CrossRef]
104. Kreitner KF, Ley S, Kauczor HU, et al. Chronic thromboembolic pulmonary hypertension: pre- and postoperative assessment with breath-hold MR imaging techniques. Radiology 2004; 232:535–543. [CrossRef]
105. Nikolaou K, Schoenberg SO, Attenberger U, et al. Pulmonary arterial hypertension: diagnosis with fast perfusion MR imaging and high-spatial-resolution MR angiography--preliminary experience. Radiology 2005; 236:694–703. [CrossRef]
106. Rajaram S, Swift AJ, Capener D, et al. Diagnostic accuracy of contrast-enhanced MR angiography and unenhanced proton MR imaging compared with CT pulmonary angiography in chronic thromboembolic pulmonary hypertension. Eur Radiol 2012; 22:310–317. [CrossRef]
107. Ley S, Ley-Zaporozhan J, Pitton MB, et al. Diagnostic performance of state-of-the-art imaging techniques for morphological assessment of vascular abnormalities in patients with chronic thromboembolic pulmonary hypertension (CTEPH). Eur Radiol 2012; 22:607–616. [CrossRef]
108. Ohno Y, Hatabu H, Murase K, et al. Primary pulmonary hypertension: 3D dynamic perfusion MRI for quantitative analysis of regional pulmonary perfusion. AJR Am J Roentgenol 2007; 188:48–56. [CrossRef]
109. Ohno Y, Koyama H, Nogami M, et al. Dynamic perfusion MRI: capability for evaluation of disease severity and progression of pulmonary arterial hypertension in patients with connective tissue disease. J Magn Reson Imaging 2008; 8:887–899. [CrossRef]